Thermodynamics and phonon dispersion of pyrope and grossular silicate garnets from ab initio simulations

Physics and Chemistry of Minerals manuscript No.
(will be inserted by the editor)

Thermodynamics and Phonon Dispersion of Pyrope and Grossular Silicate Garnets from Ab initio Simulations

Jacopo Baima · Matteo Ferrabone · Roberto Orlando · Alessandro Erba · Roberto Dovesi

Received: September 30, 2015/ Accepted: date

Abstract The phonon dispersion and thermodynamic properties of $Mg_3Al_2Si_3O_{12}$, pyrope, and $Ca_3Al_2Si_3O_{12}$, grossular, have been computed by using an *ab initio* quantum mechanical approach, an all-electron variational Gaussian type basis set and the B3LYP hybrid functional, as implemented in the CRYSTAL program. Dispersion effects in the phonon bands have been simulated by using supercells of increasing size, containing 80, 160, 320, 640, 1280 and 2160 atoms, corresponding to 1, 2, 4, 8, 16 and 27 **k** points in the first Brillouin zone. Phonon band structures, density-of-states and corresponding inelastic neutron scattering spectra are reported. Full convergence of the various thermodynamic properties, in particular entropy (S) and specific heat at constant volume (C_V), with the number of **k** points is achieved with 27 **k** points. The very regular behavior of the $S(T)$ and $C_V(T)$ curves as a function of the number of **k** points, determined by high numerical stability of the code, permits extrapolation to an infinite number of **k** points. The limiting value differs from the 27-**k** case by only 0.40% at 100 K for S (the difference decreasing to 0.11% at 1000 K) and by 0.29% (0.05% at 1000 K) for C_V. The agreement with the experimental data is rather satisfactory. We also address the problem of the relative entropy of pyrope and grossular, a still debated question. Our lattice dynamical calculations correctly describe the larger entropy of pyrope than grossular by taking into account merely vibrational contributions and without invoking "static disorder" of the Mg ions in dodecahedral sites. However, as the computed entropy difference is found to be larger than the experimental one by a factor of 2-3, present calculations can not exclude possible thermally-induced structural changes, which could lead to further conformational contributions to the entropy.

Keywords Entropy, specific heat, density functional theory, hybrid functionals, phonon density of states, inelastic neutron scattering

J. Baima · M. Ferrabone · R. Orlando · A. Erba · R. Dovesi
Dipartimento di Chimica and Centre of Excellence NIS (Nanostructured Interfaces and Surfaces), Università di Torino Via P. Giuria 5, 10125 Torino, Italy
E-mail: jacopo.baima@unito.it

1 Introduction

Garnets constitute a large class of rock forming minerals of great interest. They are fundamental not only from the technological point of view but also represent the main constituents of the Earth's lower crust, upper mantle and transition zone (Anderson 1986, 1989; Ungaretti et al. 1995). For these reasons, the accurate evaluation of the thermodynamic properties of such compounds is of great interest. Large amount of work has been carried out during the past two decades with evident progress in this field, both from the experimental and the theoretical points of view. Very accurate calorimetric measurement of the specific heat and entropy are available experimentally (Haselton and Westrum 1980; Téqui et al. 1991). Numerical estimates of such properties have also been obtained by applying a generalization of the Kieffer model (Kieffer 1979) starting from experimental vibrational frequencies at the centre of the Brillouin zone (Γ) and seismic velocities (Hofmeister and Chopelas 1991; Chopelas 2006; Ottonello et al. 1996). Such models aim at reconstructing the phonon density of states, starting from spectroscopic data in the case of optical modes, and from elastic tensors in the case of acoustic branch dispersion. From the density of states $g(\omega)$, the thermodynamic properties are calculated by means of the usual statistical mechanics relations. More accurate and detailed density of states are obtained by computing the complete phonon dispersion. Due to the size and structural complexity of this kind of minerals, most simulated phonon dispersions to date

were obtained using empirical rigid atom or shell models (Chaplin et al. 1998; Mittal et al. 2001; Gramaccioli and Pilati 2003), with few exceptions at the *ab initio* level (Wentzcovitch et al. 2010; Yu et al. 2011).

The present study shows that well converged thermodynamic properties can now be calculated *ab initio* for large unit cell complex crystal structures at a good approximation level such as the B3LYP hybrid exchange-correlation density functional. The employed method implies the use of supercells. However, it will be shown that relatively small supercells are sufficient to obtain an accurate description of the full lattice dynamics of crystals. In particular, we consider two members of the silicate garnet family, pyrope and grossular, only differing by the presence of Mg or Ca cations in the dodecahedral sites. Though containing as many as 80 atoms in the primitive unit cell, full phonon calculations for garnets can be handled by accessible computational resources, also thank to their high symmetry (I*a*3*d* cubic space group), which increases the calculation efficiency dramatically if properly used (Orlando et al. 2014; De La Pierre et al. 2014).

The possibility of computing accurate thermodynamic properties is of key importance for the correct interpretation of the experimental evidence. For example, pyrope and grossular exhibit different values of the entropy and thermal capacity because of the slight difference in their compositions. However, the observed trends are counter-intuitive and the origin of such anomalous behaviour is still debated.

It is well known experimentally that the entropy of pyrope is larger than that of grossular, which is an unexpected result since heavier Ca ions in grossular should correspond to lower vibration frequencies than for pyrope, particularly in the low-frequency range of the spectrum. Indeed, low-frequency modes are expected to contribute the most significant part of the entropy and specific heat of crystals, so that larger values of the entropy and specific heat would be expected for grossular than for pyrope. This is, however, not the case. By crystal chemistry intuition, a Mg ion can be claimed to be just "too small" for a dodecahedral site, a condition that would lead the ion to be "dynamically" or "statically" disordered, with consequences not only in the thermodynamic properties of pure pyrope and grossular, but also for the the entire range of their solid solutions, with intermediate compositions. Several authors in the literature invoke "dynamical disorder" (Gibbs and Smith 1965; Pavese et al. 1995; Kolesov and Geiger 1998; Geiger 2013) to comply with the experimental evidence, while others propose that "static disorder" only affects a "subsite" of the 24c dodecahedral site of Mg (Cressey 1981; Pilati et al. 1996; Gramaccioli and Pilati 2003). Rigid ion model simulations enable to predict the correct entropy inversion by explicitly taking into account the excess disorder entropy resulting from the displacement of Mg ions (Gramaccioli and Pilati 2003), but it should be noted that rigid ion as well as shell model calculations encounter some difficulties in dealing with the lowest part of the spectrum at Γ (Chaplin et al. 1998; Gramaccioli and Pilati 2003). Density Functional Theory (DFT) results can provide a more solid basis for the analysis and discussion of this behavior. A detailed description of the potential of Mg ions in the dodecahedral site in previous DFT studies led to exclude the possibility of static disorder (Winkler et al. 2000) and to a one-to-one comparison between the experimental and calculated vibrational frequencies (Pascale et al. 2005; Zicovich-Wilson et al. 2008). In such studies, however, the *ab initio* description of the lattice dynamics of the system was limited either to the Mg ion or to all modes at the Γ point.

By virtue of recent advances, both in the hardware and in the software, (Bush et al. 2011; Orlando et al. 2012; Dovesi et al. 2014a) *ab initio* investigation of thermodynamic properties of complex materials has become a feasible task. We show here thermodynamic data obtained for pyrope and Grossular end member garnets with the CRYSTAL14 program (Dovesi et al. 2014b) by including phonon dispersion in the direct (frozen-phonon) approach. The method consists in obtaining the vibrational spectrum in reciprocal space points other than Γ from the Hessian matrix on a supercell of the original primitive cell. How dense does a reciprocal space sampling need to be in order to achieve the calculation of well-converged thermodynamic properties? Such convergence trend is analyzed in this work as a function of the number of **k**-points used for integration in the reciprocal space. The method used implies construction of consistent supercells in each case. On this purpose, supercells of increasing size were considered, ranging from the conventional cell containing 160 atoms to one with 2160 atoms by progressively doubling the supercell size through the cases with 320, 640 and 1280 atoms.

This work is organized as follows. First, we provide the computational details about our calculations and give a brief description of the method implemented in CRYSTAL for the calculation of the phonon dispersion. Then, we discuss the convergence trend of the thermodynamic properties of pyrope as a benchmark for our method. We also illustrate and analyze phonon density-of-states and inelastic neutron scattering spectra of pyrope and grossular. Finally, we compare our result for the entropy and specific heat of pyrope and grossular to the experimental data, analyzing the problem of the higher entropy of pyrope than grossular into detail.

2 Computational details and method

Calculations were performed with the *ab initio* quantum mechanical CRYSTAL program (Dovesi et al. 2014b,a), that uses a local basis set of Gaussian-type functions, in conjunction with the hybrid B3LYP functional (Becke 1993).

Table 1 Consistency of the total energy and vibration wavenumbers of pyrope in supercells (SC) of increasing number of atoms (N) with reference to X27. ΔE is the total energy difference per formula unit (in micro-hartree); $\Delta\nu_{Max}$ and RMS (in cm^{-1}) are the maximum difference and the Root Mean Square of the full set of wavenumbers obtained in Γ. The various SCs belong to different lattice types: primitive (P), body-centered (I) and face-centered (F). s denotes the shrinking factor defining the Pack-Monkhorst net for each SC.

SC	Lattice	N	s	ΔE	$\Delta\nu_{Max}$	RMS(ν)
X1	I	80	3	1.22	0.357	0.050
X2	P	160	3	1.64	0.066	0.016
X4	F	320	2	2.15	0.032	0.009
X8	I	640	2	0.99	0.025	0.007
X16	P	1280	1	0.74	0.012	0.001
X27	I	2160	1	-	-	-

The atomic orbitals on oxygen, silicon, aluminum and magnesium were described by (8s)-(411sp)-(1d), (8s)-(6311sp)-(1d), (8s)-(611sp)-(1d) and (8s)-(511sp)-(1d) contractions, respectively. Five parameters, which were set to 7, 7, 7, 7, 16, control the truncation of the Coulomb and exchange infinite series (Dovesi et al. 2014b). We sampled reciprocal space by a regular sublattice with shrinking factor $s = 3$, corresponding to four independent $\mathbf{k}$ vectors in the irreducible wedge of the Brillouin zone for the primitive cell containing 80 atoms. The shrinking factor has progressively been reduced for larger supercells, as documented in Table 1. The exchange-correlation contribution to the Fock matrix was evaluated by numerical integration over the unit cell volume. Radial and angular points of the integration grid were generated as suitable for Gauss-Legendre radial quadrature and a Lebedev two-dimensional angular distribution. In the present work, a pruned grid with 99 radial points and a maximum of 1454 angular points was used, as obtained by using the `XXLGRID` keyword in the CRYSTAL14 manual (Dovesi et al. 2014b). Convergence threshold on the energy for the self-consistent-field (SCF) step of the calculations was set to 10^{-11} Ha for both the structure optimizations and phonon calculations.

All structures were optimized by use of analytical energy gradients with respect to both atomic coordinates and unit-cell parameters (Doll 2001; Doll et al. 2001; Civalleri et al. 2001), with a quasi-Newton technique combined with the BFGS algorithm for Hessian updating (Broyden 1970; Fletcher 1970; Goldfarb 1970; Shanno 1970). Convergence was checked on both gradient components and nuclear displacements; the corresponding tolerances on their root mean square were chosen to be 10 times more severe than the default values, that is, 0.00003 a.u. and 0.00012 a.u., respectively.

The calculation of vibration frequencies at the Γ point ($\mathbf{k} = \mathbf{0}$, the center of the First Brillouin Zone, FBZ), within the harmonic approximation, has for long been available in the CRYSTAL program. For a detailed description of the method, we refer to previous works (Pascale et al. 2004; Zicovich-Wilson et al. 2004). Here, we simply recall that they are obtained from diagonalization of the mass-weighted Hessian matrix:

$$W^{\Gamma}_{ai,bj} = \frac{H^{\mathbf{0}}_{ai,bj}}{\sqrt{M_a M_b}} \quad \text{with} \quad H^{\mathbf{0}}_{ai,bj} = \left(\frac{\partial^2 E}{\partial u^{\mathbf{0}}_{ai} \partial u^{\mathbf{0}}_{bj}} \right) , \qquad (1)$$

where E denotes the total energy per cell and atoms a and b in the reference cell, with atomic mass M_a and M_b, are displaced along the ith and jth Cartesian directions from the equilibrium configuration. First order derivatives are computed analytically, whereas second order derivatives are obtained numerically, using a two-point formula.

Calculation of the vibration frequencies of a large unit cell system such as pyrope is, in general, a resource demanding problem. The algorithm illustrated above, in principle, would require 481 SCF-plus-Gradient (SCF+G) calculations (two sets of displacements along each of three independent coordinates for each of the 80 atoms in the unit cell plus the equilibrium structure). However, symmetry reduces the set of required SCF+G runs to 17 only.

The calculation of thermodynamic properties is more demanding as it implies knowledge of the phonon dispersion inside the full FBZ. Beside $\mathbf{W}^{\Gamma}$, in this case, a set of dynamical matrices, $\mathbf{W}^{\mathbf{k}}$, need to be formed for a set of wavevectors $\mathbf{k} = \sum_i \frac{\kappa_i}{L_i} \mathbf{b}_i$ expressed as linear combinations of reciprocal lattice basis vectors $\mathbf{b}_i$ with fractional coefficients referred to shrinking factors L_i, κ_i being an integer ranging from 0 to $L_i - 1$, thus including Γ and points within the FBZ. Phonons at $\mathbf{k}$ points other than Γ can be obtained by the *direct method* (Parlinski et al. 1997; Togo et al. 2008; Alfè 2009; Erba et al. 2013), which requires the construction of supercells (SC) of the original unit cell:

$$W^{\mathbf{k}}_{ai,bj} = \sum_{\mathbf{g} \in SC} \frac{H^{\mathbf{g}}_{ai,bj}}{\sqrt{M_a M_b}} e^{\imath \mathbf{k} \cdot \mathbf{g}} . \qquad (2)$$

Indeed, equation (2) shows that each dynamical matrix in the FBZ is obtained by Fourier transforming the Hessian matrices, $\mathbf{H}^{\mathbf{g}}$, for an adequate set of real space lattice vectors $\mathbf{g}$. Lattice vectors $\mathbf{g} = \sum_i l^g_i \mathbf{a}_i$, expressed in terms of the real lattice basis vectors $\{\mathbf{a}_i\}$ through the integer coefficients l^g_i, are all contained in the SC in real space whose size and shape are determined by parameters L_i. At variance with equation (1), matrix element $H^{\mathbf{g}}_{ai,bj} = \partial^2 E / (\partial u^{\mathbf{0}}_{ai} \partial u^{\mathbf{g}}_{bj})$ refers to a displacement of atom b in cell $\mathbf{g}$ inside the SC along the Cartesian direction j, along with all its images throughout the superlattice generated by the SC. L_i are the same both in the real and the reciprocal space so as to maintain a one-to-one matching between $\mathbf{g}$ vectors in the SC and sampled $\mathbf{k}$ points. From diagonalization of the dynamical matrices the normal modes and corresponding vibration frequencies

($\nu_{\mathbf{k}p}$) are sampled over the entire FBZ. The corresponding energy levels are given by the usual harmonic expression:

$$\varepsilon_m^{p,\mathbf{k}} = \left(m + \frac{1}{2}\right)\omega_{\mathbf{k}p}\,, \tag{3}$$

where m is an integer and $\omega_{\mathbf{k}p} = 2\pi\nu_{\mathbf{k}p}$. The overall vibrational canonical partition function of a crystal, $Q_{\mathrm{vib}}(T)$, at a given temperature T, can be expressed as follows:

$$Q_{\mathrm{vib}}(T) = \frac{1}{n_k}\sum_{\mathbf{k}}\sum_{p}\sum_{m}\exp\left[-\frac{\varepsilon_m^{p,\mathbf{k}}}{k_B T}\right]\,, \tag{4}$$

where k_B is Boltzmann's constant and n_k the number of $\mathbf{k}$ points considered. According to standard statistical mechanics, thermodynamic properties of crystalline materials such as entropy, $S(T)$, and thermal contribution to the internal energy, $\mathscr{E}(T)$, can be expressed as (Erba et al. 2015e):

$$S(T) = k_B T\left(\frac{\partial \log(Q_{\mathrm{vib}})}{\partial T}\right) + k_B \log(Q_{\mathrm{vib}})\,, \tag{5}$$

$$\mathscr{E}(T) = k_B T^2\left(\frac{\partial \log(Q_{\mathrm{vib}})}{\partial T}\right)\,. \tag{6}$$

From the above expression for $\mathscr{E}(T)$, the constant-volume specific heat, $C_V(T)$, can also be computed according to $C_V(T) = \partial\mathscr{E}(T)/\partial T$. By casting equation (4) into equations (5) and (6) one gets the following harmonic expressions:

$$S(T) = k_B\sum_{\mathbf{k}p}\left[\frac{\hbar\omega_{\mathbf{k}p}}{k_B T\left(e^{\frac{\hbar\omega_{\mathbf{k}p}}{k_B T}}-1\right)} - \log\left(1-e^{-\frac{\hbar\omega_{\mathbf{k}p}}{k_B T}}\right)\right]\,, \tag{7}$$

$$C_V(T) = \sum_{\mathbf{k}p}\frac{(\hbar\omega_{\mathbf{k}p})^2}{k_B T^2}\,\frac{e^{\frac{\hbar\omega_{\mathbf{k}p}}{k_B T}}}{\left(e^{\frac{\hbar\omega_{\mathbf{k}p}}{k_B T}}-1\right)^2}\,. \tag{8}$$

This method is easily implemented, the main drawback being its computational cost, which depends on the size of the SC. However, all the SCs considered here preserve cubic symmetry, so that in all cases only 17 SCF+G calculations are needed. Because the thermodynamic properties are the result of an integration over a finite set of $\mathbf{k}$ points, convergence of the properties needs to be checked carefully by considering supercells of increasing size. On this purpose the trend of thermodynamic properties was monitored for L_i varying from 1 to 3, with the content of the corresponding SC increasing from 80 to 2160 atoms.

Let us stress that if, in principle, equation (2) could be used to compute and then diagonalize the dynamical matrices of just the $L = \prod_i L_i$ $\mathbf{k}$-points defined above, this restriction disappears when long-range electrostatic contributions to the force constants vanish within the SC. In this case, such an expression can be used to construct the dynamical matrices of a denser set of $\mathbf{k}$-points through Fourier interpolation.

Alternative approaches might also be used (and some of them have actually been used in the present study for the calculation of phonon band structures; see the Supplementary Information), which allow for computing converged thermodynamic properties of solids by keeping the size of the adopted SC relatively smaller by explicitly evaluating long-ranged electrostatic contributions to the interatomic force constants (Gonze et al. 1994; Gonze and Lee 1997; Wang et al. 2010; Baroni et al. 2001).

3 Results and discussion

3.1 Assessment of the method

As the construction of SCs is a necessary step in the application of the *direct method* to the evaluation of the thermodynamic properties of crystals, a preliminary check of the size-consistency of the method is mandatory. DFT methods are intrinsically size-consistent. However, accuracy of the results of a complex numerical procedure strongly depends on the implementation robustness and the choice of the computational parameters. Two properties that are invariant with respect to the unit cell size were considered for such a test: the total energy per formula unit and the full set of wavenumbers associated with the normal vibration modes at the Γ point. They were computed for six different SCs, namely X1, X2, X4, X8, X16 and X27, with X1 denoting the primitive cell and Xn a SC with volume n times as large as that of the primitive cell (and corresponding to a sampling of the phonon dispersion over n $\mathbf{k}$ points in the FBZ). The same set of SCs was, then, used to study the convergence of the thermodynamic properties.

The fifth column in Table 1 reports the total energy difference per formula unit (ΔE, in μHa) between X27 (the largest SC considered in this work) and the smaller SCs. In spite of the fairly large size of the SCs, the total energy per formula unit can be computed with extreme accuracy in all cases, fluctuations being in the order of the μHa. It must be remarked that the total energy is not only almost size-invariant, it is also shape-invariant as the various supercells along the series span different kinds of cubic lattices: body-centered (I), primitive (P) and face-centered (F). Similar considerations hold true also for the full set of wavenumbers at the Γ point. The two columns on the right of Table 1 give the maximum differences in the computed wavenumbers observed along the series in the range between X1 and X27 and their root mean square, with respect to X27. All such indices correspond to just a fraction of 1 cm^{-1}: a tiny uncertainty.

Within such a numerically stable framework we can confidently analyze the dependence of the thermodynamic properties on the size of the $\mathbf{k}$ point grid used for integration in the reciprocal space, so relying on the absence of spurious

effects connected to the creation of SCs that might affect our results. In particular, we refer to the thermal entropy S and specific heat at constant volume, C_V, which were evaluated at four different temperatures: 30, 100, 300 and 1000 K.

The four plots in either Figures S1 and S2 in the Supporting Information show fairly neat convergence trends of S and C_V for pyrope upon increasing the **k** point grid, despite numerical evaluation of integrals is generally not expected to be necessarily regular and monotonic (taking also into account the fact, mentioned above, that I, P and F cubic lattices are alternating when the volume increases). In such conditions it was easy to fit the data of each set to an arbitrary curve with equation $f(n_k) = a + \frac{b}{n_k} + \frac{c}{n_k^2}$ through parameters a, b and c, whose values are reported in the inset of each diagram. Computed data are better aligned to the respective fitting curves at higher temperatures. By extrapolating to the limit of an infinite supercell, X27 is estimated to yield 99.89% of S and 99.95% of C_V at 1000 K, an excellent level of convergence in both cases. Nevertheless, even at 50 K, S and C_V result to be underestimated by less than 2% with respect to their limiting values. Convergence rates are better appreciated in Figures 1 and 2 (dot-dashed lines) reporting the difference between the values of S and C_V obtained with the various supercells and the estimated asymptotic limit as a function of the temperature. It is fairly evident that X27 yields very well converged results almost irrespectively of the temperature. However, low frequency modes, which are dominant contributions to the partition function at low temperatures, appear to depend more critically on the accuracy of the integration grid (the acoustic branch varies rapidly around Γ). Slight discontinuities observed particularly for X4 and X8 may also reflect the change in the shape of the supercells from that of a face-centered to a body-centered lattice, so that it is not only the number of **k** points in the grid to change, but also the grid topology. At higher temperatures, also higher frequency modes contribute to Q and curves become progressively smoother.

3.2 Comparison with experimental thermodynamic properties: pyrope

Both S and C_V were computed in the 10-1000 K temperature range with X27, which was shown in the above section to yield very well converged properties. The experimental data are due to Haselton and Westrum (1980) for a synthetic sample of pyrope in the T range between 5 and 350 K and to Téqui et al. (1991) for $T \geq 400$ K. We obtained these latter data from the following equation (where C_P is given in J/(K mol)):

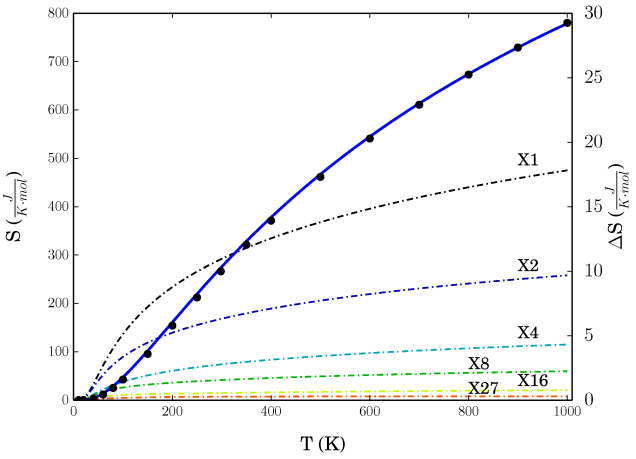

Fig. 1 Calculated (solid line, X27) and experimental (circles) entropy S of pyrope. Dash-dotted curves illustrate the convergence of the calculated entropy as a function of the number of reciprocal space **k** points used for the integration of the phonon bands. The six curves show the difference ΔS between the entropy obtained on the X1, X2, X4, X8, X16, X27 supercells and the asymptotic limit obtained by extrapolation.

$$C_P(T) = -592.635 + 138.003 \ln T + \frac{1.91204 \cdot 10^5}{T} - \frac{7.2066 \cdot 10^7}{T^2} + \frac{7.9749 \cdot 10^9}{T^3} , \quad (9)$$

which is singled out by the authors as their "preferred" fitting function of the experimental data in that range of T. Heat capacities are reported as C_P in the experimental papers. We transformed them to C_V by means of the standard anharmonic correction (Kieffer 1979; Erba 2014; Erba et al. 2015b,a,c), as suggested by Hofmeister and Chopelas (1991):

$$C_V(T) = C_P(T) - T\alpha^2(T)VK , \quad (10)$$

where the product of the volume times the bulk modulus (VK) has been considered constant with T and set to the values reported in Table 2 in Hofmeister and Chopelas (1991) along with that of the thermal expansion coefficient $\alpha(T)$. For $T \geq 400$ K, the experimental values of S were obtained as

$$S(T) = S(298.15) + \int_{298.15}^{T} \frac{C_P}{T} dT , \quad (11)$$

where $S(298.15)$ was taken from Haselton and Westrum (1980) and C_P was obtained from equation (9). Let us stress that the experimental entropy derived following this procedure is at constant-pressure whereas our computed entropy is obtained at constant-volume, a difference which could account for some slight discrepancies between the two. The *ab initio* calculation of the constant-pressure entropy would indeed require a complete quasi-harmonic treatment (Erba 2014),

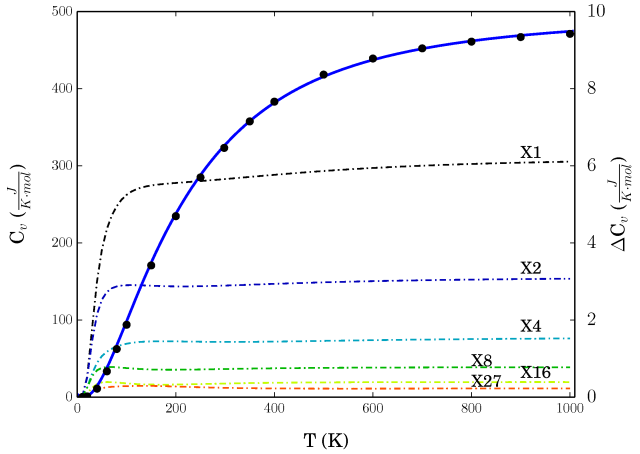

Fig. 2 Calculated (solid line, X27) and experimental (circles) heat capacity at constant volume C_V of pyrope. The plot is organized as in Figure 1.

which is behind the scope of the present investigation. Some of the present authors are currently performing such a study on six end-members of the silicate garnet family and results will be presented in a forthcoming paper.

Figures 1 and 2 show that the agreement between the calculated and the experimental data obtained from calorimetric measurements (Haselton and Westrum 1980; Téqui et al. 1991; Hofmeister and Chopelas 1991; Chopelas 2006) is remarkable: in the scale of the figure the curves of the calculated data run through the experimental points fairly well. On closer inspection, however, one sees that the two sets of data are not precisely superimposed. The differences between them (ΔS and ΔC_V) are reported in Tables S1 and S2 of the Supplementary Information. Such differences are fairly small as in no case they exceed 7.5 J/(K mol) for S and 5 J/(K mol) for C_V within the considered range of T, that is, they are about two orders of magnitudes less than the actual values of the two properties. The ΔS data show a nearly systematic trend of the calculated data to overestimate the experimental values of S, particularly in the low T range. This can be related to the well known fact that the B3LYP functional, despite its excellent overall behavior in reproducing vibrational spectra of solids, undershoots systematically low wavenumbers, roughly those below 150 cm^{-1}(Demichelis et al. 2010b; De La Pierre et al. 2011; Maschio et al. 2011; Dovesi et al. 2011; Maul et al. 2015). Indeed, common experience with B3LYP shows that this Hamiltonian describes softer structures with respect to reality, (Demichelis et al. 2010a) overestimating the lattice parameters.

Table S3 of the Supplementary Information shows that also in the case of pyrope the agreement with experimental spectra is quite good, with an overall slight underestimation of the frequencies ($\overline{\Delta\nu}$=-1.3 cm^{-1}) and a mean absolute error (MAE) of 5.7 cm^{-1}. The systematic underestimation, however, originates in the low frequency region, and taking into account only frequencies above 150 cm^{-1} the mean difference becomes 0.3 cm^{-1} and the MAE reduces to 4.5 cm^{-1}. This effect was already observed in the study of the simulated IR spectra of the six most abundant garnets (Dovesi et al. 2011), and appears only in garnets containing small cations (Mg and Fe). The low frequency vibrations in garnets are indeed dominated by motions of the cations hosted in octahedral and dodecahedral sites, as we will discuss into more detail in Section 3.3 where atomic phonon-density-of-states will be illustrated. In particular, magnesium ions in pyrope lie in a rather weak potential, which allows them to move quite freely. Mg ions give rise to a triple degenerate low frequency inactive mode, as well as a triple degenerate Raman active mode, falling in the same frequency range of the acoustic branches around the zone border. In B3LYP calculations the cage in which Mg ions move is larger than reality due to the error on the lattice parameters. Thus the frequency of the Raman active mode and likely of the inactive mode are underestimated. As belonging to the lowest frequency range, these two modes significantly contribute to thermodynamic properties, particularly at low T. Spectra computed using the experimental cell parameters instead of the optimized ones display a worse overall agreement with experiment but a much better agreement in the low frequency region, confirming the connection between the error in frequency and lattice parameter (Dovesi et al. 2011). A calculation at the experimental volume on the primitive cell reduces S by about 6% at 298 K.

Comparison of the calculated with the experimental spectra is, of course, limited to the set of modes available experimentally at Γ only, whereas the full set of modes at several **k** points contribute to the thermodynamic properties. In particular, in addition to low lying Γ modes, low energy phonons include the acoustic bands, which are directly related to the elastic properties of the system (Wallace 1972; Kieffer 1979; Dove 1993; Artioli et al. 1996). As documented in a few recent studies, where $P-V$ equations-of-state are also reported (Erba et al. 2014b,c,a; Mahmoud et al. 2014; Lacivita et al. 2014), the B3LYP elastic constants obtained for all investigated silicate garnets at *0 K* turn out to be in good agreement with experimental results obtained at *room temperature*, thus suggesting that the softening of the structures due to thermal vibrations may compensate for the systematic softening of B3LYP. This would imply that B3LYP acoustic branches have slightly lower energy with respect to the real low temperature limit.

The agreement between the calculated and experimental values of S seems to improve at higher temperature ($T >$ 400) where the low-frequency modes become less dominant. At T=1000 K ΔS becomes even negative (Table S1). However, despite one could envisage a trend of ΔS for $400 < T \leq 1000$, this cannot be considered very significant as the variation of ΔS in that range is very small and the exper-

imental values of S are affected by the form of the fitting function used (see equation 9), for which several proposals have been reported.

The behavior of C_V (Table S2) is similar to that observed for S, with a slightly better agreement of the calculated with respect to the experimental data for $T > 400$ K. In this case comparison also relies on the correctness of equation (10) for the conversion of the experimental C_P to C_V. In particular, equation (10) does not appear to be applicable to very low T such as 10 K, where a negative value is obtained for C_V, though very close to zero.

Previous computational estimates of S and C_V are based on two main strategies:

1. Properties obtained from phonon dispersion calculated with empirical rigid ion or shell models (Artioli et al. 1996; Mittal et al. 2001)
2. Properties obtained from a model phonon density of states, reconstructed from the elastic constants/seismic velocities providing information relative to the acoustic bands and from the IR-Raman vibrational data providing information about the optical branches (Hofmeister and Chopelas 1991; Chopelas 2006; Ottonello et al. 1996).

Gramaccioli and Pilati (2003), who based their calculations on strategy 1, underestimate S and C_V by as much as 30 and 14 J/(K mol), respectively, particularly at low T (see S^G(vib) in Table S1 and C_V^G(vib) in Table S2). They are able to remarkably improve the agreement with the experimental data by assuming an additional contribution to the purely thermal S and C_V due to configurational disorder (S^G(cor) and C_V^G(cor) in Tables S1 and S2) of the Mg atoms being displaced from their equilibrium positions (Haselton and Westrum 1980; Cressey 1981; Hofmeister and Chopelas 1991; Pavese et al. 1995; Mittal et al. 2001; Chopelas 2006). However, previous *ab initio* calculations provided a detailed analysis of the potential energy surface around the Mg atoms, concluding that there is no subsite dodecahedral ordering of Mg in pyrope (Winkler et al. 2000). The results from our calculations show that their model indeed undershoots S^G(vib) and C_V^G(vib). This point of view is also supported by Geiger (2013) ascribing large observed heat capacities for pyrope to "low energy phonons related to the large amplitude Mg vibrations" rather than to static disorder.

The quality of the results obtained by Hofmeister and Chopelas (1991) following strategy 2 is amazingly good, as they were able to deduce the full vibrational spectrum in Γ from a clever analysis of the available experimental data. Their estimated values of S and C_V undershoot the experimental data by just 12 and 9 J/(K mol), respectively, at most. On the basis of the results from our calculations (dot-dashed lines in Figures 1 and 2) we are able to provide a quantitative assessment of the error associated with neglecting the effects of dispersion in their model, that is, about 6 J/(K mol)

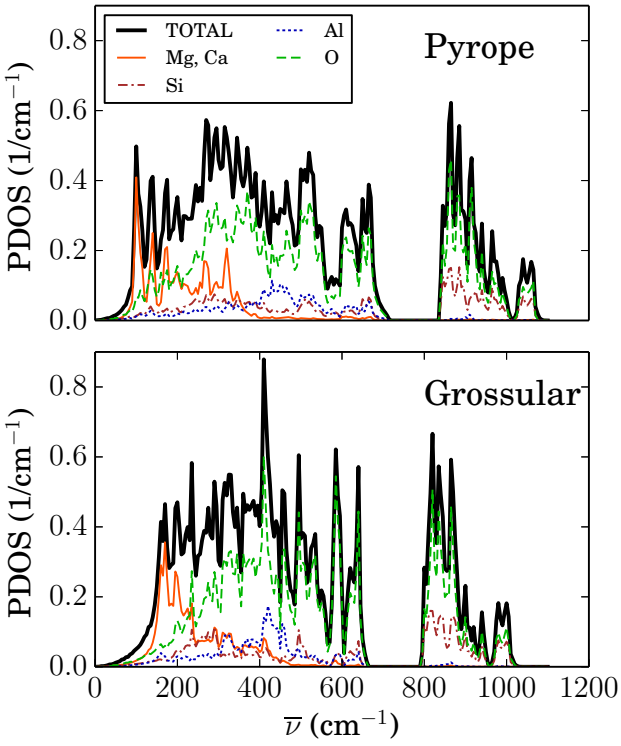

Fig. 3 (color online) Total (black continuous line) and atomic (dashed green line for O, blue dotted for Al, dark red dot-dashed for Si and continuous red for either Mg or Ca) phonon density-of-states (PDOS) for pyrope and grossular, computed on the largest supercell (X27) with additional **k** points obtained by Fourier interpolation (for a total of 13824 points).

but for very low T in the case of C_V, while the amount of the correction to S shows a stronger dependence on T and is as large as 18 J/(K mol) at $T = 1000$ K. Adding such a correction to S^H would improve the agreement with the experimental data in the lower range of T, though it would lead to overestimating data at higher T. The results obtained with a similar approach by Ottonello et al. (1996) display an even better agreement with experiments, but at the price of fitting explicitly a parameter of the model to calorimetric data at room temperature instead of deriving it from vibrational spectra.

3.3 Phonon density-of-states and inelastic neutron scattering spectra

Knowledge of the full phonon dispersion of a system also allows to compute the phonon density-of-states (PDOS) and to simulate the results of inelastic neutron scattering (INS) experiments. The total PDOS $g(\omega)$ is defined by the equation:

$$g(\omega) = \frac{1}{V_{\mathrm{BZ}}} \int_{\mathrm{BZ}} \sum_{p=1}^{3N} \delta(\omega_{\mathbf{k}p} - \omega) d\mathbf{k} \,, \qquad (12)$$

where V_{BZ} is the volume of the Brillouin zone and the integration is performed over it. From equation (12), the PDOS is normalized to $3N$, being N the number of atoms per cell ($\int g(\omega)d\omega = 3N$). The total PDOS can be partitioned into atomic contributions $g(\omega) = \sum_a g_a(\omega)x_a$ where the sum runs over the atomic species of the system, x_a is the fraction of atomic species a with respect to N, and

$$g_a(\omega) = \frac{1}{n_{\mathbf{k}}} \sum_{p,\mathbf{k}} |\mathbf{e}_{p,\mathbf{k};a}|^2 \delta(\omega_{\mathbf{k}p} - \omega) \,, \tag{13}$$

where $\mathbf{e}_{p,\mathbf{k}}$ are the eigenvectors of the dynamical matrices $W^{\mathbf{k}}$ defined in equation (2) and the integral in equation (12) has been replaced by the sum over the sampled points within the FBZ.

Total and atomic projected PDOS of both pyrope and grossular are reported in Figure 3. As previously pointed out by Mittal et al. (2001) by means of semi-empirical interatomic potential calculations, overall, the total PDOS of silicate garnets exhibit the same features for all end-members: a broad band up to about 700 cm^{-1}, a phonon band-gap of about 120 cm^{-1} and a second, sharper band above approximately 800 cm^{-1} and below about 1100 cm^{-1}. The upper band is seen to be utterly dominated by motions of the SiO_4 tetrahedra for both pyrope and grossular. The interesting part of the spectrum (particularly so for thermodynamic properties) is the low-frequency one, which is seen to be mostly affected by the motions of cations in dodecahedral sites (Mg and Ca for pyrope and grossular, respectively). By comparing the two panels of the figure, we clearly see that Mg ions in pyrope are involved in lower-frequency modes (lowest peak in the corresponding atomic PDOS at about 100 cm^{-1}) than Ca ones in grossular (lowest peak at about 180 cm^{-1}), thus confirming the picture we introduced in previous paragraphs. The complete dispersion of phonon bands of pyrope and grossular is plotted in Figures S3 and S4 of the Supplementary Information, as computed from the dynamical matrices of the largest supercell (X27) with additional $\mathbf{k}$ points obtained by Fourier interpolation along four independent paths between high-symmetry points within the FBZ.

From atomic projected PDOS, a neutron-weighted phonon density-of-states (NW-PDOS) may be defined, which can be compared to the outcomes of INS experiments:

$$g^{\mathrm{NW}}(\omega) = C \sum_a \frac{\sigma_a}{M_a} g_a(\omega) x_a \,, \tag{14}$$

where C is a normalization factor such that $\int g^{\mathrm{NW}}(\omega)d\omega = 3N$, and the weight of each atomic species a is given by the ratio of the atomic scattering cross-section σ_a and the atomic mass M_a (Osborn et al. 2001; Lucas et al. 2008). Depending on whether the inelastic scattering is coherent or incoherent, different cross-sections have to be considered, which are tabulated and available on-line (Sears 1992; Hudson 2001). In Figure 4, we report both the coherent (orange lines) and incoherent (blue lines) NW-PDOS of pyrope and grossular and we compare them with available INS experimental data: a coherent INS spectrum, normalized to $3N$ as in present calculations between 0 and 1100 cm^{-1} (that is, by neglecting the spurious spectral region above 1100 cm^{-1}, as already observed by Mittal et al. (2001)), is reported for grossular as measured by Zhao et al. (1997); coherent INS data for pyrope (Pavese et al. 1998) have not been reduced to NW-PDOS and therefore may be compared with the calculations only in terms of peak positions, shown as red bars in the pyrope panel. The agreement is very satisfactory in both cases: for pyrope on peak positions only, for grossular also on the absolute amplitude.

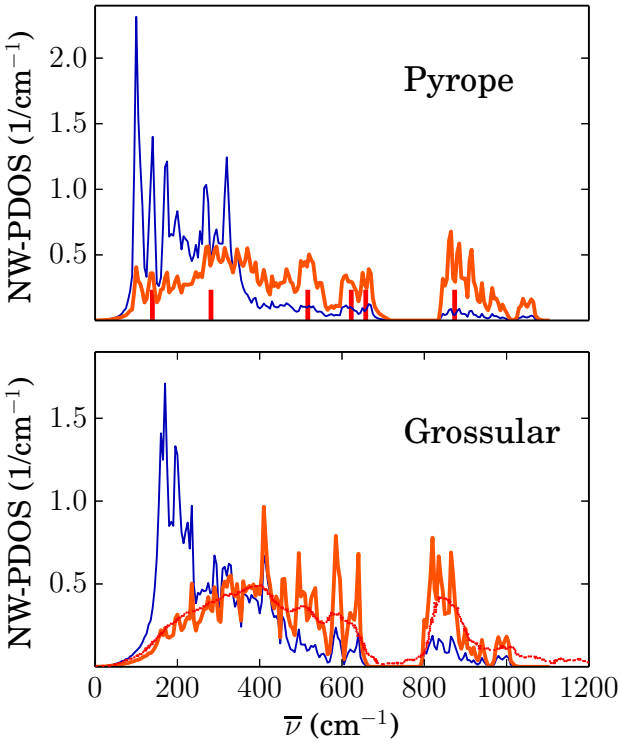

Fig. 4 (color online) Calculated incoherent (blue thin line) and coherent (thick orange line) neutron-weighted phonon density-of-states (NW-PDOS) for pyrope and grossular. Experimental data in red (INS spectrum for grossular, INS peak positions for pyrope).

By comparing Figures 3 and 4, we see that the coherent NW-PDOS does not differ much from the total PDOS, particularly so for pyrope while in grossular the only difference is a slight damping of the low-frequency region. This is due to the fact that the $\sigma_a^{\mathrm{coh}}/M_a$ ratios are very similar for Si (0.08), Al (0.06), Ca (0.07) and Mg (0.15); only O, which dominates the whole spectrum but the low-frequency range, has a larger ratio of 0.26. This is no more the case for the incoherent spectrum where the Mg or Ca ions have a $\sigma_a^{\mathrm{inc}}/M_a$ ratio of one or two orders of magnitude larger (0.003 and 0.001, respectively) than the other atomic species (0.0001 for Si, 0.00005 for O and 0.0003 for Al), thus drastically

modifying the shape of the spectrum by damping it for fr
quencies above about 400 cm^{-1}.

3.4 Relative entropy of pyrope and grossular

As anticipated in the Introduction, the entropy of pyrope
slightly larger than that of grossular. This is counter-intuitiv
because the two garnets only differ by the atomic specie
hosted in the dodecahedral site (Mg instead of Ca) and M
in pyrope is lighter than Ca in grossular. Then, one woul
expect lighter atomic species to imply higher vibration fr
quencies and lower statistical occupation of the correspon
ing harmonic oscillator energy levels. Thus, the capabilit
of reproducing such a trend is a very good test of the qualit
of a model.

The higher entropy of pyrope has generally been inte
preted as the result of a subtle order/disorder transition me
tioned in the previous section due to the small size of M
ions in dodecahedral sites. Although the equilibrium pos
tion of the ion is to be expected at the center of the dodec
hedron, the most common interpretation reported in the lite
ature invokes entropy-driven transitions occurring at low
between an ordered phase and a phase where the Mg atoms
are randomly displaced either statically or dynamically to-
wards the edges of the coordination polyhedron (Hofmeister
and Chopelas 1991; Artioli et al. 1996; Kolesov and Geiger
2000; Gramaccioli and Pilati 2003; Chopelas 2006). In fact,
lattice dynamical calculations based on rigid ion models (Pi-
lati et al. 1996; Gramaccioli and Pilati 2003) or on the recon-
struction of the density of states from IR and Raman spectra
(Hofmeister and Chopelas 1991; Chopelas 2006) could not
predict the correct trend of S of pyrope and grossular un-
less additional terms such as disorder were included in the
model.

In this study, we want to document which is the descrip-
tion of the entropy difference between pyrope and grossu-
lar when fully converged *ab initio* lattice dynamical calcula-
tions are performed, which include phonon dispersion. Hav-
ing this purpose in mind, we performed phonon dispersion
calculations on a X27 SC of grossular, which was proved
to provide well converged thermodynamic results as for py-
rope. We calculated S for grossular in the same range of tem-
peratures as for pyrope. Also in this case the experimental
data for comparison up to $T = 350$ K are taken from Hasel-
ton and Westrum (1980). For $T \geq 400$ we refer to the fitting
function for C_P obtained by Krupka et al. (1979), where C_P
is given in units of J/(K mol):

$$C_P(T) = 1633.3 - 0.7599T + \frac{9.113 \cdot 10^6}{T^2} - \frac{20783}{\sqrt{T}} + 2.669 \cdot 10^{-4} T^2 \,, \quad (15)$$

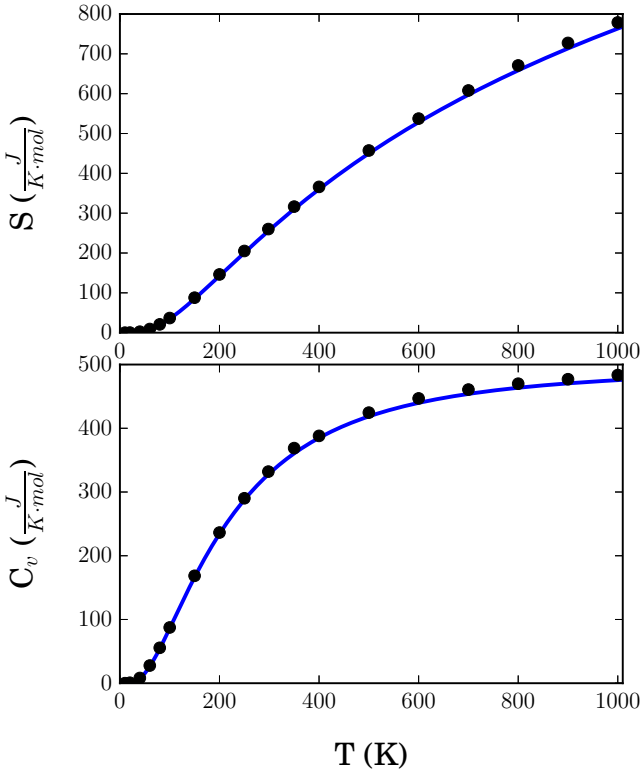

Fig. 5 Calculated (solid line, X27) and experimental (circles) heat capacity at constant volume C_V (bottom panel) and entropy S (upper panel) of grossular.

and the corresponding entropy values were calculated by equation (11). Figure 5 and table S4 of the Supplementary Information show that B3LYP generally undershoots the experimental values, only slightly in the range of low T and by as much as 15 J/(mol K) for higher T. At variance with the case of pyrope, all mode wavenumbers are predicted in good agreement with experiment. The larger size of Ca than Mg prevents the vibration modes in which Ca is involved from being affected by the tendency of B3LYP to predict softer structures than real due to steric effects.

The entropy S is also underestimated by Pilati et al. (1996) by as much as 7 J/(mol K) at the higher temperatures. On the other hand, the values of S obtained for grossular by Hofmeister and Chopelas (1991) sligthly overestimate the experimental data in the whole range of temperature where measurements were carried out (see S^H data in Table S4). Their results were obtained from vibration spectra of a natural sample, likely containing impurities of other garnets while experimental data by Haselton and Westrum (1980) and Krupka et al. (1979) were measured on a synthetic sample. Thus, there is clearly an issue about purity of samples, that must be taken into account when comparing results from different experiments and calculations. Indeed, in order to explain the discrepancy between their results and experiment, Hofmeister and Chopelas (1991) claim that the synthetic sample of grossular used in the experimental works

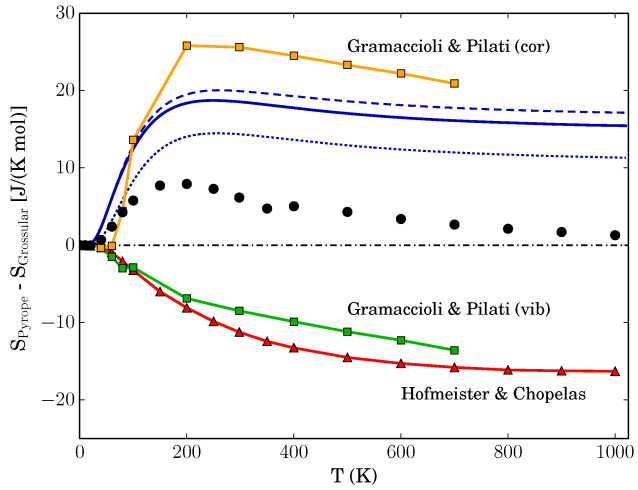

Fig. 6 Entropy difference between pyrope and grossular. Calculated (B3LYP) data are shown with a solid blue line for full phonon dispersion and with a dashed blue line for Γ only vibration frequencies; experimental data by Haselton and Westrum (1980) and Krupka et al. (1979) are given as black circles. Results from empirical models by Hofmeister and Chopelas (1991) (triangles) and Gramaccioli and Pilati (2003) and Pilati et al. (1996) (squares) are also shown for comparison. The blue dotted line represents the calculated entropy difference as obtained by calculations performed on the experimental primitive cell.

might contain a hydrogrossular component (Lacivita et al. 2015; Erba et al. 2015d), calling the attention on the fact that none of the samples used in the experimental determination corresponds to a pure grossular phase.

Availability of the two sets of data of S for pyrope and grossular allows us to compare them and verify the observed "inversion". The difference in entropy of pyrope with respect to grossular is represented in Figure 6. The experimental data (black solid circles) are affected by a slight discontinuity between $T = 350$ K and $T = 400$ K, at the conjunction of the two different sets of measurements. In the same figure, the entropy difference obtained in this study with B3LYP calculations at Γ point only (dashed blue line) and by fully converging the description of the phonon dispersion (solid blue line) are shown. While the entropy of the individual systems was previously discussed to change by as much as 18 J/(K mol) with the inclusion of a converged phonon dispersion, their difference is almost not affected at all, confirming that the entropy difference is due to lower optical frequencies at Γ point rather than to phonon dispersion in this case.

It is shown that current B3LYP calculations predict the larger entropy of pyrope as compared to grossular correctly, whereas neither the model by Hofmeister and Chopelas (1991) (triangles) nor the purely vibrational (vib) one by Gramaccioli *et al.* (Pilati et al. 1996; Gramaccioli and Pilati 2003) (squares) were accurate enough to predict the correct trend. The model by Gramaccioli *et al.* gives the correct positive entropy difference only after including an additional term assuming structural disorder of pyrope (cor), as discussed in the previous section.

Although the sign and the general trend of the relative entropy of pyrope and grossular is correctly predicted by present *ab initio* simulations, its magnitude appears to be significantly overestimated (roughly by a factor of 3 up to about 600 K and even more so above this temperature). This discrepancy might have several origins: i) the underestimation of the low-frequency optical modes (main responsible for the entropy difference) of pyrope, which are better described in the case of grossular; ii) the constant-volume constraint in the calculation of the entropy; iii) a thermally-induced static disorder in pyrope with a more complex entropy effect than a simple additive contribution.

In order to understand whether or not (and to which extent) the overestimation of the lattice parameter (and its effect on the low vibration frequencies) may be a key factor in the corresponding overestimation of the entropy difference, frequency calculations were repeated using the experimental lattice parameter for both pyrope and grossular, on their primitive cells (as the effect of phonon dispersion has been demonstrated to be negligible on the entropy difference). The obtained results are given in Figure 6 as a dotted blue line. It is seen that the entropy difference still exhibits the correct sign and has a lower magnitude even if it still overestimates the experiment. However, it must be noticed that adopting the experimental lattice parameters results in a systematic blue-shift of *all* vibration frequencies (not just of the low ones of pyrope), thus significantly deteriorating the description of the optical part of the spectrum of both systems, particularly so for grossular.

4 Conclusions

Phonon dispersion and thermodynamic properties of pyrope and grossular silicate garnets have been studied at *ab initio* level with the B3LYP hybrid density functional. A direct method has been applied involving the construction of supercells in order to obtain the phonon dispersion on a grid of reciprocal space points. The convergence of the thermodynamic properties (namely entropy and specific heat) of pyrope as a function of supercell size has been explicitly investigated, showing that a supercell containing 2160 atoms (27 times the primitive cell) ensures a very satisfactory convergence on the calculated properties. Plausible assumptions based on the nuclear masses of Mg and Ca ions suggest that the entropy of grossular should exceed that of pyrope. However, this is not observed in experimental calorimetric determination of this property on the two compounds. Previous calculations based on rigid ion models for the lattice dynamic or on the reconstruction of the phonon density of states from IR and Raman spectra failed at repro-

ducing the experimental ordering of the entropies: for this reason it was proposed in the past and widely discussed in the literature the possibility of a subtle entropy driven order-disorder transition involving the Mg ions in pyrope. These atoms are in fact located in a very soft potential due to the large size of the coordination polyhedron as compared to the radius of Mg ions themselves. Our *ab initio* calculations show that a merely vibrational analysis of the two systems as performed at the DFT level of theory with a hybrid B3LYP functional is able to correctly reproduce the larger entropy of pyrope. The absolute entropy difference, however, is overestimated by a factor of 2-3, which leaves open the possibility of static disorder being present in pyrope but playing a subtler role. The relative description of low-frequency modes in pyrope and grossular has also been discussed in terms of total and atomic projected phonon density-of-states, and of corresponding inelastic neutron scattering spectra.

References

Alfè D (2009) PHON: A program to calculate phonons using the small displacement method. Comput Phys Comm 180(12):2622–2633

Anderson DL (1986) Transition region of the earth's upper mantle. Nature 320:321–328

Anderson DL (1989) Theory of the earth. Blackwell Scientific Publications, Boston

Artioli G, Pavese A, Moze O (1996) Dispersion relations of acoustic phonons in pyrope garnet; relationship between vibrational properties and elastic constants. Am Mineral 81(1-2):19–25

Baroni S, de Gironcoli S, Corso AD, Giannozzi P (2001) Phonons and related crystal properties from density-functional perturbation theory. Rev Mod Phys 73:515

Becke AD (1993) Density-functional thermochemistry. III. The role of exact exchange. J Chem Phys 98(7):5648–5652

Broyden CG (1970) The Convergence of a Class of Double-rank Minimization Algorithms 1. General Considerations. J Inst Math Appl 6:76–90

Bush I, Tomić S, Searle B, Mallia G, Bailey C, Montanari B, Bernasconi L, Carr J, Harrison N (2011) Parallel implementation of the ab initio CRYSTAL program: electronic structure calculations for periodic systems. Proc R Soc A: Math Phys Eng Sci 467:2112–2126

Chaplin T, Price DG, Ross NL (1998) Computer simulation of the infrared and Raman activity of pyrope garnet, and assignment of calculated modes to specific atomic motions. Am Mineral 83:841

Chopelas A (2006) Modeling the thermodynamic parameters of six endmember garnets at ambient and high pressures from vibrational data. Phys Chem Min 33(6):363–376

Civalleri B, D'Arco P, Orlando R, Saunders VR, Dovesi R (2001) Hartree-Fock geometry optimization of periodic system with the CRYSTAL code. Chem Phys Lett 348:131

Cressey G (1981) Entropies and enthalpies of aluminosilicate garnets. Contrib Mineral Petr 76(4):413–419

De La Pierre M, Orlando R, Maschio L, Doll K, Ugliengo P, Dovesi R (2011) Performance of six functionals (LDA, PBE, PBESOL, B3LYP, PBE0, and WC1LYP) in the simulation of vibrational and dielectric properties of crystalline compounds. The case of forsterite Mg_2SiO_4. J Comp Chem 32(9):1775–1784

De La Pierre M, Orlando R, Ferrabone M, Zicovich-Wilson CM, Dovesi R (2014) Exploitation of symmetry in periodic Self-Consistent-Field ab initio calculations: application to large three-dimensional compounds. Sci China Chem 57(10):1418–1426

Demichelis R, Civalleri B, D'Arco P, Dovesi R (2010a) Performance of 12 DFT functionals in the study of crystal systems: Al2SiO5 orthosilicates and Al hydroxides as a case study. Int J Quantum Chem 110(12):2260–2273

Demichelis R, Civalleri B, Ferrabone M, Dovesi R (2010b) On the performance of eleven DFT functionals in the description of the vibrational properties of aluminosilicates. Int J Quantum Chem 110(2):406–415

Doll K (2001) Implementation of analytical Hartree-Fock gradients for periodic systems. Comput Phys Comm 137:74

Doll K, Harrison NM, Saunders VR (2001) Analytical Hartree-Fock gradients for periodic systems. Int J Quantum Chem 82:1

Dove MT (1993) Introduction to lattice dynamics. Cambridge University Press, Cambridge

Dovesi R, De La Pierre M, Ferrari AM, Pascale F, Maschio L, Zicovich-Wilson CM (2011) The IR vibrational properties of six members of the garnet family: A quantum mechanical ab initio study. Am Mineral 96(11-12):1787–1798

Dovesi R, Orlando R, Erba A, Zicovich-Wilson CM, Civalleri B, Casassa S, Maschio L, Ferrabone M, De La Pierre M, D'Arco P, Nol Y, Caus M, Rrat M, Kirtman B (2014a) CRYSTAL14: A program for the ab initio investigation of crystalline solids. Int J Quantum Chem 114(19):1287–1317

Dovesi R, Saunders VR, Roetti C, Orlando R, Zicovich-Wilson CM, Pascale F, Doll K, Harrison NM, Civalleri B, Bush IJ, D'Arco P, Llunell M, Causà M, Noël Y (2014b) `CRYSTAL14` User's Manual. Università di Torino, Torino, http://www.crystal.unito.it

Erba A (2014) On combining temperature and pressure effects on structural properties of crystals with standard ab initio techniques. J Chem Phys 141:124,115

Erba A, Ferrabone M, Orlando R, Dovesi R (2013) Accurate dynamical structure factors from ab initio lattice dynamics: The case of crystalline silicon. J Comput Chem 34:346

Erba A, Mahmoud A, Belmonte D, Dovesi R (2014a) High Pressure Elastic Properties of Minerals from Ab initio Simulations: The Case of Pyrope, Grossular and Andradite Silicate Garnets. J Chem Phys 140:124,703

Erba A, Mahmoud A, Orlando R, Dovesi R (2014b) Elastic properties of six silicate garnet end members from accurate ab initio simulations. Phys Chem Min 41(2):151–160

Erba A, Mahmoud A, Orlando R, Dovesi R (2014c) Erratum to: Elastic Properties of Six Silicate Garnet End-members from Accurate Ab initio Simulations. Phys Chem Min 41:161–162

Erba A, Maul J, De La Pierre M, Dovesi R (2015a) Structural and Elastic Anisotropy of Crystals at High Pressure and Temperature from Quantum-mechanical Methods: The Case of Mg_2SiO_4 Forsterite. J Chem Phys 142:204,502

Erba A, Maul J, Demichelis R, Dovesi R (2015b) Assessing Thermochemical Properties of Materials through Ab initio Quantum-mechanical Methods: The Case of α-Al_2O_3. Phys Chem Chem Phys 17:11,670–11,677

Erba A, Maul J, Itou M, Dovesi R, Sakurai Y (2015c) Anharmonic Thermal Oscillations of the Electron Momentum Distribution in Lithium Fluoride. Phys Rev Lett 115:117402

Erba A, Navarrete-López AM, Lacivita V, D'Arco P, Zicovich-Wilson CM (2015d) Katoite under Pressure: An Ab initio Investigation of its Structural, Elastic and Vibrational Properties Sheds Light on the Phase Transition. Phys Chem Chem Phys 17:2660–2669

Erba A, Shahrokhi M, Moradian R, Dovesi R (2015e) On How Differently the Quasi-harmonic Approximation Works for Two Isostructural Crystals: Thermal Properties of Periclase and Lime. J Chem Phys 142:044,114

Fletcher R (1970) A new approach to variable metric algorithms. Comput J 13(3):317–322

Geiger CA (2013) Static disorders of atoms and experimental determination of Debye temperature in pyrope: Low- and high-temperature single-crystal X-ray diffraction study – Discussion. Am Mineral 98:780–782

Gibbs GV, Smith JV (1965) Refinement of the crystal structure of synthetic pyrope. Am Mineral 50:2032–2039

Goldfarb D (1970) A Family of Variable-Metric Methods Derived by Variational Means. Math Comput 24:23–26

Gonze X, Lee C (1997) Dynamical matrices, born effective charges, dielectric permittivity tensors, and interatomic force constants from density-functional perturbation theory. Phys Rev B 55:10,355

Gonze X, Charlier JC, Allan D, Teter M (1994) Interatomic force constants from first principles: The case of α-quartz. Phys Rev B 50:13,035–13,038

Gramaccioli CM, Pilati T (2003) Interpretation of Single-Crystal Vibrational Spectra and Entropy of Pyrope and Almandine Using a Rigid-Ion Lattice-Dynamical Model. J Phys Chem A 107(22):4360–4366

Haselton H Jr, Westrum E Jr (1980) Low-temperature heat capacities of synthetic pyrope, grossular, and $pyrope_{60}$ $grossular_{40}$. Geochim Cosmochim Acta 44(5):701–709

Hofmeister AM, Chopelas A (1991) Thermodynamic properties of pyrope and grossular from vibrational spectroscopy. Am Mineral 76(5-6):880–891

Hudson BS (2001) Inelastic Neutron Scattering: A Tool in Molecular Vibrational Spectroscopy and a Test of ab Initio Methods. J Phys Chem A 105(16):3949–3960

Kieffer SW (1979) Thermodynamics and lattice vibrations of minerals: 3. Lattice dynamics and an approximation for minerals with application to simple substances and framework silicates. Rev Geophys 17(1):35–59

Kolesov BA, Geiger CA (1998) Raman spectra of silicate garnets. Phys Chem Min 25(2):142–151

Kolesov BA, Geiger CA (2000) Low-temperature single-crystal Raman spectrum of pyrope. Phys Chem Min 27(9):645–649

Krupka KM, Robie RA, Hemingway BS (1979) High-temperature heat capacities of corundum, periclase, anorthite, $CaAl_2Si_2O_8$ glass, muscovite, pyrophyllite, $KAlSi_3O_8$ glass, grossular, and $NaAlSi_3O_8$ glass. Am Mineral 64(1-2):86–101

Lacivita V, Erba A, Dovesi R, D'Arco Ph (2014) Elasticity of Grossular-Andradite Solid Solution: An Ab initio Investigation. Phys Chem Chem Phys 16:15,331–15,338

Lacivita V, Mahmoud A, Erba A, D'Arco P, Mustapha S (2015) Hydrogrossular, $Ca_3Al_2(SiO_4)_{3-x}(H_4O_4)_x$: An Ab initio Investigation of its Structural and Energetic Properties. Am Mineral DOI: 10.2138/am-2015-5334

Lucas MS, Kresch M, Stevens R, Fultz B (2008) Phonon partial densities of states and entropies of Fe and Cr in bcc Fe-Cr from inelastic neutron scattering. Phys Rev B 77:184,303

Mahmoud A, Erba A, Doll K, Dovesi R (2014) Pressure Effect on Elastic Anisotropy of Crystals from Ab initio Simulations: The Case of Silicate Garnets. J Chem Phys 140:234,703

Maschio L, Ferrabone M, Meyer A, Garza J, Dovesi R (2011) The infrared spectrum of spessartine $Mn_3Al_2Si_3O_{12}$: An ab initio all electron simulation with five different functionals (LDA, PBE, PBESOL, B3LYP and PBE0). Chemical Physics Letters 501(4):612–618

Maul J, Erba A, Santos IMG, Sambrano JR, Dovesi R (2015) In silico infrared and Raman spectroscopy under pressure: The case of $CaSnO_3$ perovskite. J Chem Phys 142(1):014,505

Mittal R, Chaplot SL, Choudhury N (2001) Lattice dynamics calculations of the phonon spectra and thermodynamic properties of the aluminosilicate garnets pyrope, grossular, and spessartine $M_3Al_2Si_3O_{12}$ (M = Mg, Ca, and Mn). Phys Rev B 64:094,302

Orlando R, Delle Piane M, Bush IJ, Ugliengo P, Ferrabone M, Dovesi R (2012) A new massively parallel version of CRYSTAL for large systems on high performance computing architectures. J Comp Chem 33(28):2276–2284

Orlando R, De La Pierre M, Zicovich-Wilson CM, Erba A, Dovesi R (2014) On the full exploitation of symmetry in periodic (as well as molecular) self-consistent-field ab initio calculations. J Chem Phys 141(10):104,108

Osborn R, Goremychkin EA, Kolesnikov AI, Hinks DG (2001) Phonon Density of States in MgB_2. Phys Rev Lett 87:017,005

Ottonello G, Bokreta M, Sciuto PF (1996) Parametrization of Energy and Interactions in Garnets: End-member Properties. Am Mineral 81:429–447

Parlinski K, Li ZQ, Kawazoe Y (1997) First-Principles Determination of the Soft Mode in Cubic ZrO_2. Phys Rev Lett 78:4063–4066

Pascale F, Zicovich-Wilson CM, Gejo FL, Civalleri B, Orlando R, Dovesi R (2004) The calculation of the vibrational frequencies of the crystalline compounds and its implementation in the CRYSTAL code. J Comp Chem 25:888–897

Pascale F, Zicovich-Wilson CM, Orlando R, Roetti C, Ugliengo P, Dovesi R (2005) Vibration Frequencies of $Mg_3Al_2Si_3O_{12}$ Pyrope. An ab Initio Study with the CRYSTAL Code. J Phys Chem B 109(13):6146–6152

Pavese A, Artioli G, Prencipe M (1995) X-ray single-crystal diffraction study of pyrope in the temperature range 30-973 K. Am Mineral 80(5-6):457–464

Pavese A, Artioli G, Moze O (1998) Inelastic neutron scattering from pyrope powder: experimental data and theoretical calculations. Eur J Mineral 10(1):59–70

Pilati T, Demartin F, Gramaccioli CM (1996) Atomic displacement parameters for garnets: a lattice-dynamical evaluation. Acta Crystallogr Sec B 52(2):239–250

Sears V (1992) Neutron scattering lengths and cross sections. Neutron News 3(3):29–37

Shanno DF (1970) Conditioning of Quasi-Newton Methods for Function Minimization. Math Comput 24:647–656

Téqui C, Robie RA, S Hemingway B, R Neuville D, Richet P (1991) Melting and thermodynamic properties of pyrope ($Mg_3Al_2Si_3O_{12}$). Geochim Cosmochim Acta 55(4):1005–1010

Togo A, Oba F, Tanaka I (2008) First-principles calculations of the ferroelastic transition between rutile-type and CaCl2-type SiO2 at high pressures. Phys Rev B 78:134,106

Ungaretti L, Leona M, Merli M, Oberti R (1995) Non-ideal solid-solution in garnet; crystal-structure evidence and modelling. Eur J Mineral 7:1299–1312

Wallace D (1972) Thermodynamics of crystals. Wiley, New York.

Wang Y, Wang J, Wang Y, Mei ZG, Shang SL, Chen LQ, Liu ZK (2010) A mixed-space approach to first-principles calculations of phonon frequencies for polar materials. J Phys: Condens Matter 22:202,201

Wentzcovitch RM, Yu YG, Wu Z (2010) Thermodynamic Properties and Phase Relations in Mantle Minerals Investigated by First Principles Quasiharmonic Theory. Rev Mineral Geochem 71:59–98

Winkler B, Milman V, Akhmatskaya EV, Nobes RH (2000) Bonding and dynamics of Mg in pyrope: a theoretical investigation. Am Mineral 85(3-4):608–612

Yu YG, Wentzcovitch RM, Vinograd VL, Angel RJ (2011) Thermodynamic properties of $MgSiO_3$ majorite and phase transitions near 660 km depth in $MgSiO_3$ and Mg_2SiO_4: A first principles study. J Geophys Res 116:B02,208

Zhao J, Gaskell P, Cormier L, Bennington S (1997) Vibrational density of states and structural origin of the heat capacity anomalies in Ca_3 Al_2 Si_3 O_{12} glasses. Phys B 241:906–908

Zicovich-Wilson CM, Pascale F, Roetti C, Orlando VRSR, Dovesi R (2004) The calculation of the vibration frequencies of α-quartz: the effect of Hamiltonian and basis set. J Comput Chem 25:1873–1881

Zicovich-Wilson CM, Torres FJ, Pascale F, Valenzano L, Orlando R, Dovesi R (2008) Ab initio simulation of the IR spectra of pyrope, grossular, and andradite. J Comp Chem 29(13):2268–2278